Internal Stresses Lead to Net Forces and Torques on Extended Elastic Bodies

Hillel Aharoni,[1,2] John M. Kolinski,[1] Michael Moshe,[1,3,4] Idan Meirzada,[1] and Eran Sharon[1,*]
[1]The Racah Institute of Physics, The Hebrew University of Jerusalem, Jerusalem 91904, Israel
[2]Department of Physics & Astronomy, University of Pennsylvania, Philadelphia, Pennsylvania 19104, USA
[3]Department of Physics, Soft matter program, Syracuse University, Syracuse, New York 13244, USA
[4]Department of Physics, Harvard University, Cambridge, Massachusetts 02138, USA
(Received 23 May 2016; published 16 September 2016)

A geometrically frustrated elastic body will develop residual stresses arising from the mismatch between the intrinsic geometry of the body and the geometry of the ambient space. We analyze these stresses for an ambient space with gradients in its intrinsic curvature, and show that residual stresses generate effective forces and torques *on the center of mass* of the body. We analytically calculate these forces in two dimensions, and experimentally demonstrate their action by the migration of a non-Euclidean gel disc in a curved Hele-Shaw cell. An extension of our analysis to higher dimensions shows that these forces are also generated in three dimensions, but are negligible compared to gravity.

DOI: 10.1103/PhysRevLett.117.124101

Geometrical frustration occurs when the geometry of a confining space prevents an extended system from being at its local ground state at every point; examples abound in physics, including glasses and the antiferromagnetic Ising model on a triangular lattice [1]. When an elastic body undergoes differential growth [2], swelling [3], or thermal expansion [4], it might become frustrated. This occurs when its intrinsic geometry is non-Euclidean, a geometry which is incompatible with the ambient 3D Euclidean geometry. This incompatibility leads to the accumulation of residual stresses whose magnitude depends both on the extent of incompatibility and on the dimensions of the body [5]. Frustrated solids that are not perfectly elastic can relax their frustration via changes in their intrinsic geometry, namely, by generating inelastic deformations. For example, a flat crystalline sheet constrained to a spherical shell must be strained; however, it can reduce its elastic energy by nucleating defects [6–11] (while the forces acting on such defects arise from a mismatch between the intrinsic geometry of the defect and the geometry of the embedding space, there is no change to the body's center of mass). These defects change the intrinsic geometry of the sheet to more closely match the shell's geometry, thus reducing the geometrical frustration and therefore the residual energy.

It was recently shown that structural defects in crystalline solids experience an effective "geometrical force," which is derived from the residual energy [12]. For example, disclinations in a hexagonal 2D lattice that is confined to a curved 2D surface experience a force [13], which is the derivative of the residual elastic energy with respect to the position of the defect. However, the effective force exerted upon structural defects does not imply a change in the momentum of the extended body. Instead, their resultant motion or acceleration can be accomplished by rearrangement of internal degrees of freedom within the body. In this Letter, we show that residual stresses might accumulate into net forces and torques acting on an *extended body* as a result of the presence of gradients in the curvature of the ambient space.

Geometrical frustration is naturally described within the framework of incompatible elasticity. In this framework, an elastic body is modeled as an N-dimensional (ND) Riemannian manifold, equipped with a reference metric $\bar{g}$ that represents local equilibrium distances between material elements. A configuration is an embedding of the body manifold into an ambient ND manifold. Every configuration of the body induces on the body manifold a metric g, which we call the actual metric. The elastic strain is the deviation of g from $\bar{g}$. The elastic model is fully determined by a constitutive relation, which relates the internal stresses to the strain field. In the case of a hyperelastic material, the constitutive relation can be defined by an energy functional, which is an additive measure of a local energetic cost of the strain.

Considering first the case of a 2D sheet embedded in a 2D surface; the local 2D geometry of both the sheet and embedding surface is determined by one scalar field—the Gaussian curvature. We denote the intrinsic Gaussian curvature of the sheet $\bar{K}(\boldsymbol{r})$, and the Gaussian curvature of the embedding surface $K(\boldsymbol{r})$. If $\bar{K} = K$ everywhere, then the sheet and the surface are compatible, and the sheet can adopt a stress free configuration within the surface. Geometrical frustration occurs when $\bar{K} \neq K$. In such a case parts of the sheet must be stretched or compressed in order to fit into the confining surface.

We consider a disc of radius R with a constant intrinsic curvature $\bar{K}$ embedded in a plane with spatially varying curvature. Focusing on the dominant effect, we take $R \ll K(\boldsymbol{r})/|\vec{\nabla}K|$ so that the curvature of the embedding surface

may be considered uniform across the disc, and is equal to the confining curvature at the disc's center. We now compute the total residual energy of the disc as a function of its position $\boldsymbol{r}$ for given values of $\bar{K}$, K, and R. We apply here a variation of the method of the Incompatible Stress Function (ISF) that we recently introduced [14].

The equilibrium equation for the stress tensor in the disc $\sigma^{\mu\nu}$ takes the form

$$\bar{\nabla}_\mu \sigma^{\mu\nu} + (\Gamma^\nu_{\alpha\beta} - \bar{\Gamma}^\nu_{\alpha\beta})\sigma^{\alpha\beta} = 0 \tag{1}$$

Here, Γ and $\bar{\Gamma}$ are the Christoffel symbols associated with the actual and reference metrics, respectively, and $\bar{\nabla}$ is the covariant derivative with respect to the reference metric $\bar{g}$ of the disc. As an equation for the actual metric g, Eq. (1) is a highly nonlinear equation. Nonetheless, the solution for the stress can be represented using a single scalar function ψ that is the ISF

$$\sigma^{\mu\nu} = \frac{1}{\sqrt{\det g}} \frac{1}{\sqrt{\det \bar{g}}} \varepsilon^{\mu\alpha}\varepsilon^{\nu\beta}\nabla_\alpha \bar{\nabla}_\beta \psi, \tag{2}$$

where ε is the antisymmetric Levi-Civita symbol. We can formulate simple linear equations for the ISF by adding to the small gradient assumption a small incompatibility assumption, namely,

$$R\sqrt{|K - \bar{K}|} \ll 1. \tag{3}$$

Under this assumption the representation of the stress reduces to a simpler, approximated form

$$\sigma^{\mu\nu} = \frac{1}{\det \bar{g}} \varepsilon^{\mu\alpha}\varepsilon^{\nu\beta}\bar{\nabla}_\alpha \bar{\nabla}_\beta \psi. \tag{4}$$

At this stage, we can express the actual metric in terms of the reference metric and the ISF for a Hookean disc. For plane stress problems the equation for the ISF arises from the compatibility condition $\mathrm{Gauss}(g) = 0$; i.e., the Gaussian curvature vanishes everywhere. Here we generalize this compatibility condition and require

$$\mathrm{Gauss}(g) = K. \tag{5}$$

A direct calculation of the Gaussian curvature associated with the actual metric obtained from this requirement yields an equation for the ISF ψ,

$$-\frac{1}{Y}\bar{\Delta}\,\bar{\Delta}\,\psi - \frac{2}{Y}\bar{K}\,\bar{\Delta}\,\psi + \bar{K} = K, \tag{6}$$

where Y is the 2D Young's modulus and $\bar{\Delta}$ is the Laplace-Beltrami operator associated with $\bar{g}$. The left-hand side in this equation describes the curvature associated with the energy minimizing configuration. The right-hand side describes the curvature associated with the ambient space. Equation (6) is similar to the biharmonic equation obtained for the Airy stress function in plane-stress problems; it generalizes it to arbitrary intrinsic and ambient Gaussian curvatures.

Equation (6) is accompanied with boundary conditions on the stresses. The normal stresses at the boundary should vanish, i.e., $\sigma^{\rho\rho}(R) = 0$, $\sigma^{\rho\theta}(R) = 0$, where ρ, θ are the polar coordinates on the disc. In addition, the stresses at the origin should converge to a finite value. The solution of Eq. (6) that satisfies these conditions is

$$\psi(\rho) = \frac{Y}{4\bar{K}}\left(\frac{K}{\bar{K}} - 1\right)\left(2\,\mathrm{atanh}\left(\cos(\sqrt{\bar{K}}\rho)\right) + 2\ln\left|\sin(\sqrt{\bar{K}}\rho)\right| - \cos(\sqrt{\bar{K}}\rho)\sec\left(\frac{\sqrt{\bar{K}}R}{2}\right)^2\right). \tag{7}$$

The stresses and the elastic energy stored in the disc can be directly calculated from the ISF. Since we are interested in small bodies, we can expand the residual energy in orders of R and obtain

$$E = \frac{\pi Y}{384}(K - \bar{K})^2 R^6 + \mathrm{O}(R^8). \tag{8}$$

Equation (8) indicates that for a curvature difference $\delta K(\boldsymbol{r}) \equiv \bar{K} - K(\boldsymbol{r})$, the residual elastic energy scales as $E(\boldsymbol{r}) \propto R^6(\delta K(\boldsymbol{r}))^2$; here, the change in energy, which generates the force, is only in the residual elastic energy of the disc. One notes immediately that if $\vec{\nabla}K \neq 0$ the gradient of the energy is not zero; in this case a force $\vec{F} = -\vec{\nabla}E(\boldsymbol{r})$ acts on the center of mass of the disc. Therefore, geometrical forces can act not only on virtual "geometrical charges," but also on extended elastic bodies. A condition for such forces is a nonvanishing gradient in the Gaussian curvature of the embedding surface.

In order to test whether the embedding of a frustrated disc results in forces and motion of the disc, we construct an experimental system consisting of an elastic disc with a tunable intrinsic reference metric, and a curved Hele-Shaw cell formed from two plates with a radially dependent Gaussian curvature, as shown in profile in Fig. 1(a). The discs are fabricated from P-NIPA gels, where the NIPA concentration can be varied to enable the temperature responsivity of the material, as described elsewhere [3]. When heated above $T_C \sim 33\,^\circ\mathrm{C}$ these discs shrink differentially, and can adopt a temperature dependant non-Euclidean reference metric. We cast the gel disc with a thickness of approximately 0.5 mm. The reference Gaussian curvature of the disc is varied up to $|\bar{K}|_{\max} \approx 1/4\ \mathrm{cm}^{-2}$. This temperature responsive gel disc takes on spontaneous curvature when in free space; however, when confined in the cell it can no longer assume its intrinsic geometry, and must conform to the local shape dictated by the cell.

The surfaces of the Hele-Shaw cell are axisymmetric, and follow a radial profile described by $z(r) = 5e^{-r^2/25}$ cm. As r increases, the Gaussian curvature of the Hele-Shaw

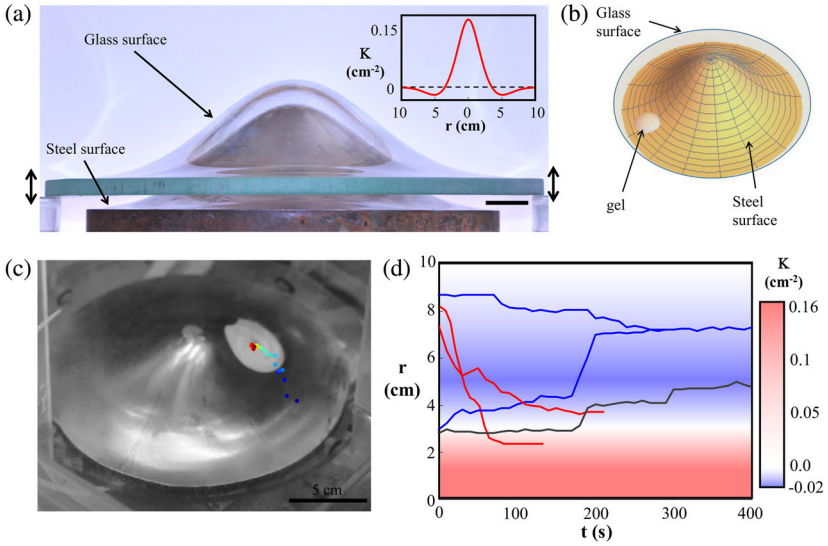

FIG. 1. Experimental schematic and demonstration of migration of a 2D frustrated gel. (a) A picture of the confining plates of the cell. Arrows indicate periodic forcing of the gap at 5 Hz using a shaker. The exaggerated gap shows how the plates form the curved Hele-Shaw cell. Scalebar: 2 cm). The cell's Gaussian curvature K is plotted as a function of radius (inset). (b) An oblique schematic view of the setup: arrows indicate the gel, the glass surface and the steel surface. This setup is immersed in a temperature-regulated water bath; by controlling the temperature, we can manipulate the intrinsic curvature of the gel. (c) A gel with positive spontaneous curvature migrates from the lower portion of the cell, where $\boldsymbol{K}(\boldsymbol{r}) < 0$, to the upper portion, where $\boldsymbol{K}(\boldsymbol{r}) > 0$. The gel is shown in its final, stable position, where it has ceased migration. The dots trace out the trajectory of the gel, where the color corresponds to time from start (blue) to finish (red). Scale bar: 5 cm (d) Several trajectories for gels with different values of reference curvature are plotted against time, with background color indicating the local value $\boldsymbol{K}(\boldsymbol{r})$. The gels with spontaneous negative curvature (blue curves) both migrate to a point near the lowest value of the local curvature. Two examples of a gel with positive spontaneous curvature (red lines) show their propagation against gravity to regions of $\boldsymbol{K}(\boldsymbol{r}) > 0$. A flat gel (dark gray) migrates to the zero in the bell. Each gel is approximately 5 cm in diameter, and thus the precision with which the gels migrate is approximately 2 cm.

cell $K(r)$ varies from positive to negative values and finally to 0, as plotted in the inset to Fig. 1(a). The Hele-Shaw cell forms a gap of 0.75 mm maintained by a suspension system with a compliance of $\sim$0.5 mm, so that at its narrowest, the disc fits tightly within the cell. The compliance enables harmonic driving of the gap at typical frequencies of 5 Hz with a shaker to prevent the gel from sticking to the surfaces; the assembly is shown schematically in Fig. 1(b). The cell-gel system is immersed in a temperature-regulated water bath. The temperature of the water can be slowly changed at a rate of $\sim 1\,^{\circ}\mathrm{C}/\,\mathrm{min}$ to allow swelling and deswelling of the gel to its equilibrium volume at any given temperature; this enables precise control over the gel's reference curvature $\bar{K}(T)$. The density of the gel is typically 1200 $\mathrm{kg/m^3}$; therefore, gel discs sink in pure water. Though density matching additives can be added to counteract the buoyancy force, as described elsewhere [15], the experiments described in this Letter were conducted in pure water. In addition, the dimensions of the disc imply a Föppl–von-Kármán number $\gamma > 100$, assuring the dominance of stretching effects with respect to bending effects. A careful calculation would show that this small bending induced force acts in the same direction as gravity, pulling the disc away from the center of the cell.

We place the discs within the cell where the Gaussian curvature of the gel and cell do not agree. A gel with $\bar{K} > 0$ is shown migrating from the region with negative Gaussian curvature to the region with positive Gaussian curvature, where it remains at equilibrium [Fig. 1(c)]. We observe migration for negatively curved gels, positively curved gels, and flat gels [Fig. 1(d)]; see the Supplemental Material [16] for examples of gel migration.

We varied the location where we initially place the gel to probe how different mismatches between $K(r)$ and $\bar{K}$ affect the gel's migration. For example, a gel with $\bar{K} < 0$ migrates from the cell's region of $K(r) = 0$ at its periphery and also from the cell's positive Gaussian curvature near its center, as shown by the two traces plotted in blue in Fig. 1(d); it migrates to precisely the same location when placed above that location and below it, both with and against the effect of gravity, respectively.

The temperature dependence of $\bar{K}$ can be used to externally control the motion of a single disc within the cell. To demonstrate this, we use a gel that has positive Gaussian curvature at high-T and a lesser Gaussian curvature as T decreases; this gel is flat at room temperature, as shown schematically in Fig. 2(a). We introduce this disc near the edge of the cell, wait until it reaches its equilibrium location in the cell, and subsequently cool the bath over a period of several minutes. Initially the temperature exceeds the critical temperature, and the disc migrates from the boundary of the cell upward, against gravity.

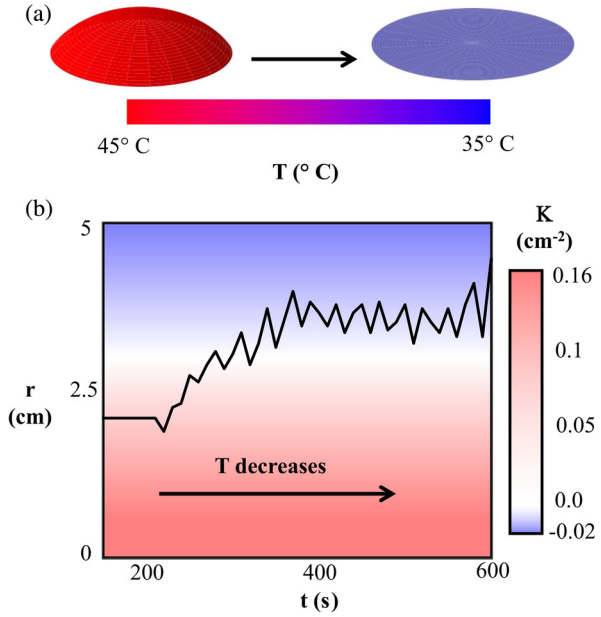

FIG. 2. Frustration driven migration of a gel with temperature-dependent intrinsic curvature. (a) The NIPA gel is cast such that it will change the value of its spontaneous curvature in response to changes in the temperature of the bath: here, the gel changes its spontaneous curvature from positive at high-temperatures to approximately flat at lower temperatures. (b) The gel is embedded in the cell at $r = 5$ cm, where the local curvature is negative, while the water bath is at 45 °C. The gel migrates upward, as shown in the red curves of Fig. 1(d). At $t = 150$ s, we begin the cooling cycle, and the water bath temperature drops to approximately 35 °C over 2 min, and the gel's spontaneous curvature is now near zero; as the bath cools, the gel simultaneously migrates down the bell to more closely match this curvature, where it remains for the remainder of the experiment.

Eventually it comes to a rest near the center of the cell, where $K(\boldsymbol{r})$ most closely matches $\bar{K}(T)$, and stays there as long as $T > T_C$. Upon further decrease of the bath's temperature, the gel migrated from the region of $K > 0$ to a region of the cell with $K = 0$, as shown in Fig. 2(b); this only occurred after the bath has cooled by several degrees. The gel remained in this location for the final 400 sec of the experiment. Frictional forces significantly overdamp the dynamics of the gel, as can be seen by the approach of the gel to its final position in each of the traces of the gel's position in Figs. 1(d) and 2(b), thus preventing quantitative comparison between the theory and the experiment, as discussed in detail in the Supplemental Material [16].

In the experiment, the forces that push the disc are obviously generated by the cell surfaces. These forces include friction or adhesion forces, which oppose the center-of-mass motion but do not generate it, and normal forces exerted perpendicularly to the mold. Since these forces are normal to the plane of the disc at every point, they do not change the in-plane stresses in the disc; these stresses are identical to those that would be obtained if the system were truly 2D. They generate a center-of-mass acceleration that does not depend on the thickness of the gel in the thin limit (both stretching forces and inertia are linear in the thickness), and is nonzero within our approximation if and only if $\vec{\nabla} K \neq 0$. It is therefore evident that these net center-of-mass forces arise from a truly 2D effect that exists regardless of an embedding in a 3D space, even though in an embedded system it is manifested via normal forces.

The forces we discuss here arise from a geometric incompatibility between the intrinsic geometry of an elastic body and the inhomogeneous geometry of its embedding space. Though the analytical solution and experimental demonstration consider a 2D body in a 2D space, all the arguments we presented also hold for higher spatial dimensions. Therefore, under certain conditions, we predict net forces acting on elastic bodies in the 3D space around us. What are these conditions? When considering a Euclidean space, it was already argued [17,18] that residually stressed 3D elastic bodies are those whose 3D reference metric is non-Euclidean. In such a space no net forces or torques will be exerted, thanks to the translational and rotational space symmetries ($\vec{\nabla} K = 0$ in our 2D analog). However, according to general relativity our space is neither truly Euclidean nor homogeneous, in which case elasticity should be formulated in a way that takes into account the nontrivial geometry of space [19]. In such a scenario, certain elastic bodies "better fit" certain curved regions in space, and we predict net forces pushing them towards those regions.

The magnitude of the residual elastic energy for an N-dimensional (ND) body in an ND space can be estimated from scaling arguments to be of the form

$$E \propto YV(K - \bar{K})^2 R^4 + O(VR^6), \tag{9}$$

where Y is an ND elastic modulus, V is the volume of the ND body ($V \propto R^N$), and K, $\bar{K}$ represent the Riemann curvature tensors of the ambient space and the reference metric, respectively. For $N = 2$ we get $E \propto Y(K - \bar{K})^2 R^6 + O(R^8)$, as we obtained from the direct analytical calculation above. However, unlike two dimensions where the curvature tensors can be written in terms of one scalar field (the Gaussian curvature), for $N > 2$ the tensors K, $\bar{K}$ have more than one independent local degree of freedom and may be locally anisotropic. The residual energy may therefore depend on orientation and thus exert geometrical torques on the body, and not just net force, even in the point-curvature approximation. For extended bodies, higher order terms may induce torque already in two dimensions, provided that both the intrinsic and ambient geometry are anisotropic. At $N = 1$, no effect is expected.

As an example, we shall look at a 3D Euclidean elastic sphere put in a Schwarzschild background. The

space components of a Schwarzschild metric are given in spherical coordinates (r, θ, φ) by

$$g_{\mathrm{sch}}^{\mathrm{spatial}} = \begin{pmatrix} (1-\frac{R_s}{r})^{-1} & 0 & 0 \\ 0 & r^2 & 0 \\ 0 & 0 & r^2\sin^2\theta \end{pmatrix}, \quad (10)$$

where R_s is the Schwarzschild radius. This leads to a nontrivial space curvature tensor with radial component $-R_s/r^3$ and angular components $R_s/2r^3$. A Euclidean elastic sphere of radius R embedded in a Schwarzschild background will therefore possess residual elastic energy of order $E \propto YVR_s^2R^4/r^6$, creating an effective repulsive force between the sphere and the massive center of the Schwarzschild metric $F_{\mathrm{el}} \approx YVR_s^2R^4/r^7$. This effect is very small compared to the force exerted on such a body by the gravitational field in the Newtonian approximation. This may be estimated as $F_g = \rho VR_sc^2/2r^2$ (with ρ, c the mass density and speed of light, respectively), and therefore the ratio between the two forces is

$$\frac{F_{\mathrm{el}}}{F_g} \approx \left(\frac{c_s}{c}\right)^2\left(\frac{R}{r}\right)^4\left(\frac{R_s}{r}\right), \quad (11)$$

where c_s is the speed of sound in the material. This expression shows that for any realistic scenario, the geometrical forces are completely negligible compared to gravitation.

In this work we showed that an elastic body can exert force and torque on itself by manipulating intrinsic degrees of freedom, much like in the tales of Baron Munchausen. This unique feature results from the explicit coupling between the reference geometry of the body and the geometry of space (which can be inhomogeneous) via incompatible elasticity. Though reminiscent of the motion of proteins on a curved membrane [20] or migration of insects near a meniscus [21], this principle depends only on the intrinsic geometries of the body and the confining space. It is not yet clear whether examples of the Munchausen effect exist outside the laboratory. We have shown that in the context of gravitation this effect is negligible. However, nature might exploit such a mechanism in biological contexts, allowing membranelike organisms to migrate on curved surfaces solely by altering their intrinsic geometry, without exerting tangential forces.

This work was supported by "SoftGrowth" project of the European Research Council. J. M. K. and M. M. acknowledge the Fulbright-Israel post-doctoral fellowship. H. A. was supported by the National Science Foundation (NSF) Grant No. DMR12-62047. H. A., M. M., and E. S. acknowledge the Kavli Institute for Theoretical Physics, UCSB.

*erans@vms.huji.ac.il

[1] G. H. Wannier, Antiferromagnetism. The Triangular Ising Net, Phys. Rev. **79**, 357 (1950).
[2] A. Goriely and M. Ben Amar, Differential Growth and Instability in Elastic Shells, Phys. Rev. Lett. **94**, 198103 (2005).
[3] Y. Klein, E. Efrati, and E. Sharon, Shaping of Elastic Sheets by Prescription of Non-Euclidean Metrics, Science **315**, 1116 (2007).
[4] A. Yuse and M. Sano, Transition between crack patterns in quenched glass plates, Nature (London) **362**, 329 (1993).
[5] E. Efrati, E. Sharon, and R. Kupferman, The metric description of elasticity in residually stressed soft materials, Soft Matter **9**, 8187 (2013).
[6] M. J. Bowick and L. Giomi, Two-dimensional matter: order, curvature and defects, Adv. Phys. **58**, 449 (2009).
[7] G. M. Grason and B. Davidovitch, Universal collapse of stress and wrinkle-to-scar transition in spherically confined crystalline sheets, Proc. Natl. Acad. Sci. U.S.A. **110**, 12893 (2013).
[8] W. T. M. Irvine, V. Vitelli, and P. M. Chaikin, Pleats in crystals on curved surfaces, Nature (London) **468**, 947 (2010).
[9] P. Lipowsky, M. J. Bowick, J. H. Meinke, D. R. Nelson, and A. R. Bausch, Direct visualization of dislocation dynamics in grain-boundary scars, Nat. Mater. **4**, 407 (2005).
[10] V. N. Manoharan, Colloidal spheres confined by liquid droplets: Geometry, physics, and physical chemistry, Solid State Commun. **139**, 557 (2006).
[11] B. L. Mbanga, G. M. Grason, and C. D. Santangelo, Frustrated Order on Extrinsic Geometries, Phys. Rev. Lett. **108**, 017801 (2012).
[12] V. Koning and V. Vitelli, Crystals and liquid crystals confined to curved geometries, arXiv:1401.4957.
[13] W. T. Irvine and V. Vitelli, Geometric background charge: dislocations on capillary bridges, Soft Matter **8**, 10123 (2012).
[14] M. Moshe, E. Sharon, and R. Kupferman, Elastic interactions between two-dimensional geometric defects, Phys. Rev. E **92**, 062403 (2015).
[15] H. Aharoni and E. Sharon, Direct observation of the temporal and spatial dynamics during crumpling, Nat. Mater. **9**, 993 (2010).
[16] See Supplemental Material at http://link.aps.org/supplemental/10.1103/PhysRevLett.117.124101 for movies of gel discs migrating within a curved Hele-Shaw cell, and discussion of experimental details.
[17] E. Efrati, E. Sharon, and R. Kupferman, Elastic theory of unconstrained non-Euclidean plates, J. Mech. Phys. Solids **57**, 762 (2009).
[18] A. Yavari, A Geometric Theory of Growth Mechanics, J. Nonlinear Sci. **20**, 781 (2010).
[19] W. C. Hernandez, Elasticity Theory in General Relativity, Phys. Rev. D **1**, 1013 (1970).
[20] J. Zimmerberg and M. M. Kozlov, How proteins produce cellular membrane curvature, Nat. Rev. Mol. Cell Biol. **7**, 9 (2006).
[21] J. W. Bush and D. L. Hu, WALKING ON WATER: Biolocomotion at the Interface, Annu. Rev. Fluid Mech. **38**, 339 (2006).